

Breaking the Data Barrier: Robust Few-Shot 3D Vessel Segmentation using Foundation Models

Kirato Yoshihara^{1,2}, Yohei Sugawara², Yuta Tokuoka², and Lihang Hong²

¹ The University of Osaka

² Preferred Networks, Inc.

kiratoyoshihara@gmail.com, {suga, tokuoka, rihankoo}@preferred.jp

Abstract. State-of-the-art vessel segmentation methods typically require large-scale annotated datasets and suffer from severe performance degradation under domain shifts. In clinical practice, however, acquiring extensive annotations for every new scanner or protocol is unfeasible. To address this, we propose a novel framework leveraging a pre-trained Vision Foundation Model (DINOv3) adapted for volumetric vessel segmentation. We introduce a lightweight 3D Adapter for volumetric consistency, a multi-scale 3D Aggregator for hierarchical feature fusion, and Z-channel embedding to effectively bridge the gap between 2D pre-training and 3D medical modalities, enabling the model to capture continuous vascular structures from limited data. We validated our method on the TopCoW (in-domain) and Lausanne (out-of-distribution) datasets. In the extreme few-shot regime with 5 training samples, our method achieved a Dice score of 43.42%, marking a 30% relative improvement over the state-of-the-art nnU-Net (33.41%) and outperforming other Transformer-based baselines, such as SwinUNETR and UNETR, by up to 45%. Furthermore, in the out-of-distribution setting, our model demonstrated superior robustness, achieving a 50% relative improvement over nnU-Net (21.37% vs. 14.22%), which suffered from severe domain overfitting. Ablation studies confirmed that our 3D adaptation mechanism and multi-scale aggregation strategy are critical for vascular continuity and robustness. Our results suggest foundation models offer a viable cold-start solution, improving clinical reliability under data scarcity or domain shifts.

Keywords: Foundation Models · Domain Generalization · Label-efficient Learning

1 Introduction

Accurate segmentation of cerebrovascular structures is critical for diagnosing neurovascular diseases, planning stent placement, and managing intracranial aneurysms [11, 19, 14]. Despite the success of standard supervised deep learning in medical image analysis, state-of-the-art approaches, such as nnU-Net [7], rely heavily on large-scale, high-quality annotated datasets. In clinical practice,

however, acquiring extensive voxel-level annotations for every new scanner, protocol, or modality is prohibitively labor-intensive and requires expert radiological knowledge [18]. This dependency creates a fundamental cold-start problem: deploying medical AI models in a new clinical center often requires collecting and annotating a significant amount of data from scratch, which is operationally unfeasible.

Existing solutions for data-efficient learning, such as Few-Shot Learning [13] and Unsupervised Domain Adaptation [8, 3], have attempted to mitigate this burden. However, standard supervised CNNs like nnU-Net tend to overfit severely when trained on extremely limited data (e.g., 5 samples), losing their generalization capability. Furthermore, they suffer from catastrophic performance degradation under out-of-distribution (OOD) shifts, where differences in imaging physics (e.g., MRI field strength, voxel spacing) cause the model to fail on unseen data [4, 23]. While Transformer-based architectures like SwinUNETR [5] offer better global context, they typically require even larger datasets to converge, exacerbating the data scarcity issue.

To address these challenges, we propose a novel framework that adapts a pre-trained 2D Vision Foundation Model (DINOv3 [16]) for robust 3D vessel segmentation. While recent foundation model adaptations like MedSAM [10] or SAM-Med3D [20] have shown remarkable success in general-purpose segmentation, our approach is designed to effectively capture complex 3D topological structures, such as sparse and thin vessels [14, 15], even under extreme data scarcity. We validate our method on the TopCoW dataset as the in-domain (ID) benchmark and the Lausanne dataset for out-of-distribution (OOD) evaluation.

Our main contributions are summarized as follows:

1. We propose a robust few-shot segmentation framework leveraging DINOv3, providing a viable solution to the medical AI cold-start problem where only a handful of annotations are available.
2. We introduce a specialized 3D adaptation mechanism consisting of Z-channel embedding to encode depth information, a multi-scale 3D Aggregator to capture vessels of varying thicknesses, and a lightweight 3D Adapter to recover volumetric context, effectively bridging the gap between 2D pre-training and 3D medical modalities.
3. We validate our method on the TopCoW (ID) and Lausanne (OOD) datasets. Our approach outperforms the state-of-the-art nnU-Net by 30% in the 5-shot regime and demonstrates superior robustness with a 50% relative improvement in OOD settings.

2 Method

2.1 Overview of the Framework

As illustrated in Fig. 1(a), our framework adapts a pre-trained 2D DINOv3 [16] for 3D segmentation via a side-tuning design [24]. Given an input volume $X \in \mathbb{R}^{B \times 2 \times D \times H \times W}$, a frozen backbone Φ_{frozen} and a 3D Aggregator \mathcal{A}_{agg} extract

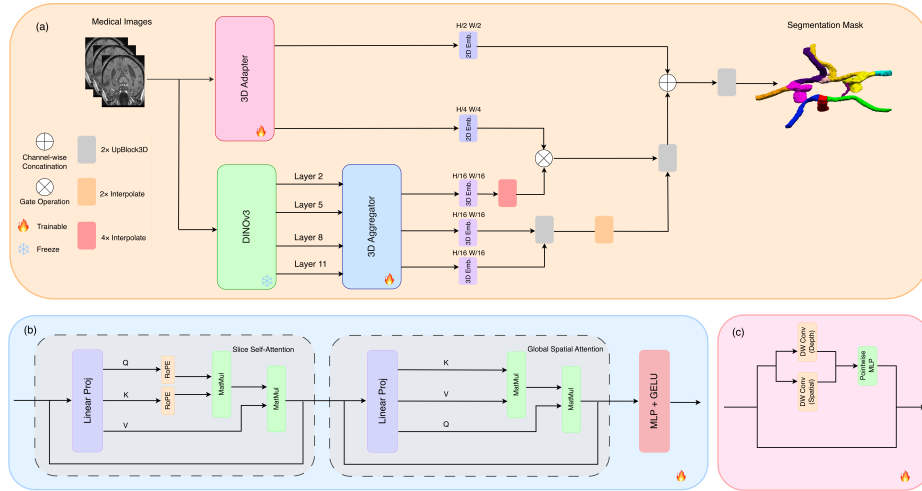


Fig. 1. Overview of the proposed framework. (a) The overall architecture leverages a frozen 2D DINOv3 backbone to extract semantic features, while a parallel Lightweight 3D Adapter captures high-frequency volumetric details. (b) The 3D Aggregator fuses these multi-scale features via factorized slice and global spatial attention. (c) The decoupled convolution block within the 3D Adapter efficiently models spatial and interslice dependencies.

global semantic context $F_{sem} = \mathcal{A}_{agg}(\Phi_{frozen}(\mathcal{T}(X)))$, where $\mathcal{T}(\cdot)$ applies slice-wise pseudo-coloring. In parallel, a trainable 3D Adapter Ψ_{train} captures high-frequency volumetric details $F_{spat} = \Psi_{train}(X)$ directly from the raw input. The final prediction $\hat{Y} \in \mathbb{R}^{B \times 1 \times D \times H \times W}$ is generated by fusing these features via a gated mechanism and passing them to the decoder \mathcal{D}_{dec} :

$$\hat{Y} = \mathcal{D}_{dec}(\text{Gate}(F_{sem}, F_{spat})) \quad (1)$$

By freezing Φ_{frozen} and updating only the lightweight modules (Ψ_{train} , \mathcal{A}_{agg} , and \mathcal{D}_{dec}), we effectively mitigate the risk of overfitting in few-shot scenarios.

2.2 Z-channel Embedding for 3D Awareness

Since the 2D DINOv3 lacks volumetric awareness, we employ an explicit Z-channel embedding to encode spatial location. We formulate the input with two channels: normalized intensity (I_{gray}) and a relative depth map (Z_{map}). To adapt this to the backbone’s RGB requirement, we construct a slice-wise pseudo-color input X_{DINO} by assigning I_{gray} to the R/G channels and Z_{map} to the B channel:

$$X_{DINO} = \text{Norm}_{\text{ImageNet}}(\text{Concat}(I_{gray}, I_{gray}, Z_{map})) \quad (2)$$

This parameter-free transformation preserves texture features via the first two channels while explicitly embedding geometric depth in the third, ensuring consistent 3D context without overfitting.

2.3 Shared Axial Aggregator and Multi-scale Fusion

To integrate multi-level semantic context, we propose the Shared Axial Aggregator (labeled as 3D Aggregator in Fig. 1(b)). It processes feature maps $\mathcal{F} = \{F^{(l)} \mid l \in \{2, 5, 8, 11\}\}$ extracted from the frozen backbone. To model 3D dependencies efficiently, we employ a weight-sharing block with factorized attention, inspired by the Alternating-Attention design in VGGT [21]. Specifically, as detailed in Fig. 1(b), we decompose the operation into Slice Self-Attention (MSA_{Slice}) with RoPE [17] to capture inter-slice continuity, followed by Global Spatial Attention (MSA_{Global}) to aggregate intra-slice semantic context:

$$H^{(l)} = MSA_{Global}(MSA_{Slice}(F^{(l)})) \quad (3)$$

Finally, the aggregated features are hierarchically upsampled and fused with the high-resolution adapter features F_{spat} via a gated mechanism:

$$F_{out} = \text{Up}(H^{(l)}) + \sigma(W_{gate} \cdot \text{Concat}(\text{Up}(H^{(l)}), F_{spat})) \odot F_{spat} \quad (4)$$

where σ is the sigmoid function and W_{gate} is a learnable convolution. This gating adaptively balances semantic priors with high-frequency spatial details.

2.4 Lightweight 3D Adapter

To recover volumetric context and high-frequency details, we introduce a parallel 3D CNN branch constructed from Anisotropic ConvNeXt Blocks [9], as detailed in Fig. 1(c). Instead of computationally heavy 3D convolutions, we decompose the depthwise stage into parallel spatial and depth-wise branches. Formally, for an input x_{in} , the depthwise output x_{dw} is:

$$x_{dw} = \text{DWConv}_{3 \times 7 \times 7}(x_{in}) + \text{DWConv}_{3 \times 1 \times 1}(x_{in}) \quad (5)$$

The first term captures spatial context, while the second models inter-slice dependencies. This is followed by a pointwise stage with a residual connection:

$$x_{out} = \text{PW}_2(\text{GELU}(\text{PW}_1(\text{LN}(x_{dw})))) + x_{in} \quad (6)$$

where PW denotes $1 \times 1 \times 1$ convolution. This decoupled design efficiently extracts multi-scale features (F_{spat}) at 1/2 and 1/4 resolutions for fusion.

3 Experiments and Results

3.1 Datasets and Implementation Details

Datasets. We validate our framework on two public cerebrovascular datasets, utilized in accordance with their open-access licenses without requiring additional IRB approval.

TopCoW (ID): We use the TopCoW challenge dataset [22], which contains 125 MRA volumes with voxel-level annotations. The dataset is split into training

($N = 87$), validation ($N = 25$), and internal test ($N = 13$) sets. To simulate a data-scarce scenario, we train using only 5 randomly sampled volumes from the training set.

Lausanne (OOD): For OOD evaluation, we employ the Lausanne dataset (OpenNeuro ds003949) [2] ($N = 128$ TOF-MRA, aneurysm patients). Lacking manual segmentation, we binarized the probabilistic atlas [12] at an empirically optimized 0.2 threshold to preserve Circle of Willis connectivity. For fair evaluation, we restricted the ground truth to a central 60% ROI, strictly matching TopCoW’s physical Field-of-View.

Implementation. The framework was implemented in PyTorch on a single NVIDIA A100 GPU. We used a frozen ViT-S/16 DINOv3 backbone (pre-trained on LVD-1689M) with trainable adapter and decoder heads, optimized using a compound loss function of Soft Dice and Cross-Entropy. Input volumes were resized to 336×336 spatially and randomly cropped to 64 depth slices, with standard augmentations (rotation, scaling, intensity shift) applied.

Baseline Configurations. We compare our method against 3D U-Net [1], SwinUNETR [5], UNETR [6], and nnU-Net (v2) [7]. To ensure a fair few-shot comparison, we standardized input resolutions (336×336) and augmentations across all methods.

Model Efficiency. We employed the ViT-S/16 distilled variant of DINOv3 (21.6M parameters) as the frozen backbone. Notably, thanks to our efficient side-tuning design, the number of trainable parameters is limited to only 13.6M. This is significantly more parameter-efficient compared to fully fine-tuning state-of-the-art 3D Transformers such as UNETR (122.3M) and SwinUNETR (62.2M), or even the standard nnU-Net (30.8M). This compact trainable footprint acts as a strong regularizer, mitigating the risk of overfitting in data-scarce regimes.

3.2 Quantitative Analysis

In-domain Performance (TopCoW). We evaluated segmentation performance across training regimes ranging from extreme few-shot ($N = 5$) to full supervision ($N = 87$). As illustrated in Fig. 2, our framework demonstrates remarkable label efficiency. In the critical 5-shot setting, our method achieves a Dice score of 43.42%, significantly outperforming the strong baseline nnU-Net (33.41%). This corresponds to a 30.0% relative improvement, highlighting the robustness of the frozen DINOv3 representations against overfitting. Other transformer baselines (SwinUNETR: 31.78%, UNETR: 30.00%) struggle to generalize, underscoring the difficulty of learning 3D representations from scratch with sparse annotations.

Capacity-Efficiency Trade-off. We observe a performance cross-over as data availability increases. In the high-data regime ($N \geq 44$), nnU-Net eventually surpasses our method (75.24% vs. 52.26% at $N = 87$). This behavior illustrates a fundamental trade-off: while our side-tuning strategy acts as a powerful regularizer in data-scarce scenarios, fully fine-tuned models like nnU-Net possess higher capacity to exploit domain-specific nuances when abundant annotations are available. Thus, our framework is uniquely positioned as an optimal solution

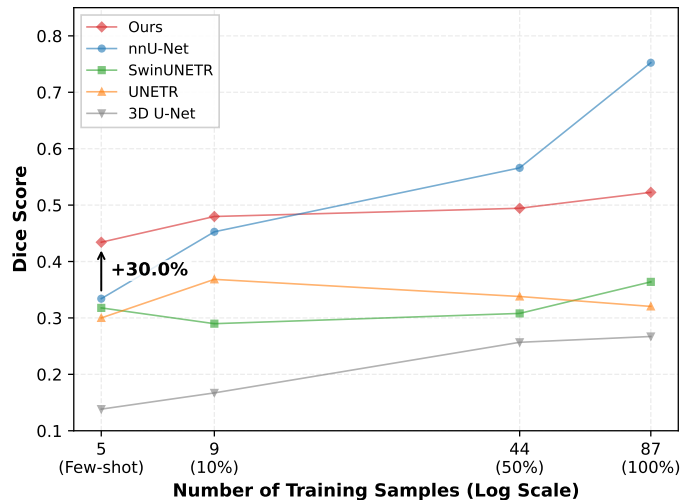


Fig. 2. Label efficiency analysis on the TopCoW (ID) dataset. We plot the Dice score (test set) against the number of training samples (log scale). Our method (red) demonstrates superior performance in the few-shot regime ($N \leq 9$), achieving a 30.0% relative improvement over nnU-Net at 5 samples. Furthermore, our method consistently outperforms all other baselines (SwinUNETR, UNETR, 3D U-Net) by a substantial margin across all data regimes, as these models fail to generalize even with full supervision ($< 40\%$ Dice). While nnU-Net recovers capacity in the high-data regime, our approach remains the most robust solution under label scarcity.

for cold-start medical segmentation tasks where collecting large-scale annotations is prohibitive.

Quantitative Analysis on the OOD dataset. To assess generalization, we evaluated models trained on TopCoW (ID) directly on the unseen Lausanne dataset (OOD). Table 1 confirms that our method consistently outperforms nnU-Net across all data regimes. In the challenging 5-shot setting, our approach achieved a 50.3% relative improvement in Dice and a 58.4% gain in topological connectivity (cIDice). This indicates that the frozen DINOv3 backbone provides a robust generic prior, enabling superior transferability compared to features learned from scratch. Crucially, while increasing source training data caused nnU-Net to overfit (stagnant Dice, worsening HD95), our method continued to improve, widening the performance gap to a 63.8% relative advantage in the fully supervised setting. These results demonstrate that our side-tuning strategy effectively mitigates overfitting to source-domain nuances, preserving robustness where conventional models fail.

3.3 Qualitative Analysis

Visual comparisons on the external Lausanne dataset (OOD) are presented in Fig. 3. To rigorously assess cross-domain robustness, we randomly selected a

Table 1. Cross-domain generalization results on the Lausanne dataset (OOD). Our method outperforms nnU-Net in all metrics across all data regimes. While nnU-Net degrades in shape fidelity (HD95 increases) as training data increases, our method maintains robust performance, highlighting the generalizability of the frozen backbone.

Data	nnU-Net			Ours		
	Dice(%) \uparrow	clDice \uparrow	HD95(mm) \downarrow	Dice(%) \uparrow	clDice \uparrow	HD95(mm) \downarrow
5-shot	14.22	0.053	22.61	21.37	0.084	15.94
10%	14.89	0.051	24.37	17.19	0.076	16.45
50%	11.23	0.037	31.25	24.05	0.108	14.21
100%	13.74	0.057	29.03	22.50	0.095	15.77

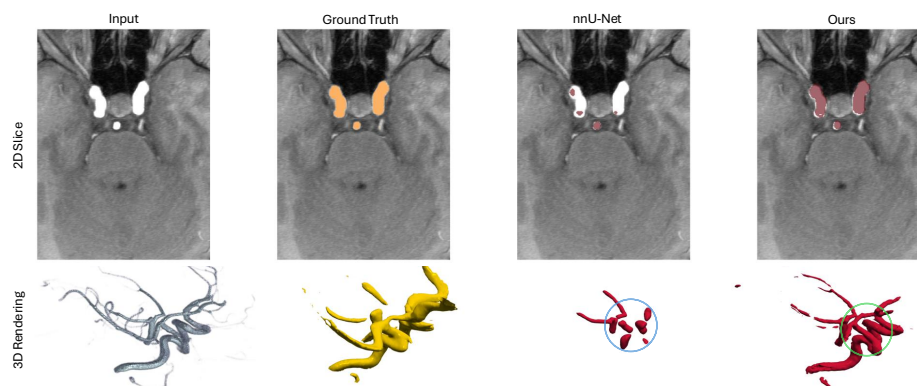


Fig. 3. Qualitative comparison on the unseen OOD Lausanne dataset (trained on 5 TopCoW subjects). Samples were randomly selected to ensure unbiased evaluation. Top Row: A 2D slice where nnU-Net fails due to domain shift, while our method correctly delineates the vessel. Bottom Row: 3D rendering of a different subject; the baseline produces fragmented results (blue circle), while our method preserves vascular connectivity (green circle).

sample and utilized models trained on only 5 samples from the TopCoW (ID) dataset.

Robustness to Domain Shift (2D View). Fig. 3(Top Row) displays representative 2D slices. As shown, the baseline nnU-Net struggles to generalize to the target domain, failing to detect the vascular structure evident in the input. This indicates that standard supervised learning inevitably overfits to the ID intensity distribution when training data is scarce. In contrast, our method accurately identifies the vessel boundaries. This demonstrates that the frozen DINOv3 backbone captures domain-invariant features rather than relying solely on intensity statistics, thereby maintaining performance even under significant distribution shifts.

Topological Integrity (3D View). The limitation of the baseline is further amplified in the 3D reconstructions in Fig. 3(Bottom Row). Due to the lack of

Table 2. Ablation study on the TopCoW dataset (5-shot). We evaluate the contribution of key components: 3D Adapter, 3D Aggregator, Multi-scale fusion, and Z-channel. The full model yields the best balance of volumetric overlap (Dice%) and topological preservation (clDice), while maintaining boundary accuracy (HD95) within 1.5 mm of the best variant.

Method	Dice(%) \uparrow	clDice \uparrow	HD95(mm) \downarrow
w/o 3D Aggregator	22.35	0.279	60.97
w/o 3D Adapter	28.67	0.072	85.33
Only Last Layer (11)	42.88	0.284	53.37
Only Last Layer (11) w/o Z	41.10	0.304	52.87
Ours (Full)	43.42	0.310	54.29

robust 2D detection, nnU-Net generates severe discontinuities and isolated fragments (blue circle). Conversely, our approach successfully preserves the topological connectivity of the vessel tree (green circle). This confirms that our multi-scale aggregation strategy not only improves pixel-level accuracy but also maintains global structural coherence, validating the effectiveness of our approach for downstream clinical tasks that rely on vascular continuity.

3.4 Ablation Study

Table 2 validates our design choices. Removing the 3D Adapter or 3D Aggregator caused catastrophic performance drops, confirming that naively applying a 2D backbone is insufficient for volumetric data. Furthermore, comparisons against the single-scale baseline demonstrate that both our multi-scale aggregation and Z-channel embedding are essential for improving segmentation accuracy and maintaining topological connectivity.

4 Discussion and Conclusion

In this study, we addressed the challenge of label-efficient volumetric segmentation by adapting a frozen 2D pre-trained DINOv3 backbone. Our experiments demonstrated that this strategy acts as a powerful regularizer, significantly outperforming fully supervised baselines in few-shot regimes and showing superior robustness against domain shifts where standard models overfit.

While fully fine-tuned models eventually surpass our method with abundant data due to the capacity limits of a frozen backbone, our approach effectively breaks the dependency on large-scale annotations. We conclude that bridging 2D pre-trained foundation models with lightweight 3D components offers a viable, robust cold-start solution for clinical deployment, enhancing reliability even with scarce data or varying protocols.

References

1. Çiçek, Ö., Abdulkadir, A., Lienkamp, S.S., Brox, T., Ronneberger, O.: 3d u-net: learning dense volumetric segmentation from sparse annotation. In: International conference on medical image computing and computer-assisted intervention. pp. 424–432. Springer (2016)
2. Di Noto, T., Marie, G., Tourbier, S., Alemán-Gómez, Y., Esteban, O., Saliou, G., Cuadra, M.B., Hagmann, P., Richiardi, J.: Towards automated brain aneurysm detection in TOF-MRA: Open data, weak labels, and anatomical knowledge. *Neuroinformatics* **21**, 21–34 (2023). <https://doi.org/10.1007/s12021-022-09597-0>
3. Dou, Q., Ouyang, C., Chen, C., Chen, H., Glocker, B., Zhuang, X., Heng, P.A.: Pnp-adanet: Plug-and-play adversarial domain adaptation network at unpaired cross-modality cardiac segmentation. *Ieee Access* **7**, 99065–99076 (2019)
4. Guan, H., Liu, M.: Domain adaptation for medical image analysis: A survey. *IEEE Transactions on Biomedical Engineering* **69**, 1173–1185 (2022). <https://doi.org/10.1109/TBME.2021.3117407>
5. Hatamizadeh, A., Nath, V., Tang, Y., Yang, D., Roth, H.R., Xu, D.: Swin unetr: Swin transformers for semantic segmentation of brain tumors in mri images. In: International MICCAI brainlesion workshop. pp. 272–284. Springer (2021)
6. Hatamizadeh, A., Tang, Y., Nath, V., Yang, D., Myronenko, A., Landman, B., Roth, H.R., Xu, D.: Unetr: Transformers for 3d medical image segmentation. In: Proceedings of the IEEE/CVF winter conference on applications of computer vision. pp. 574–584 (2022)
7. Isensee, F., Jaeger, P.F., Kohl, S.A.A., Petersen, J., Maier-Hein, K.H.: nnu-net: a self-configuring method for deep learning-based biomedical image segmentation. *Nature Methods* **18**, 203–211 (2021). <https://doi.org/10.1038/s41592-020-01008-z>
8. Kamnitsas, K., Baumgartner, C., Ledig, C., Newcombe, V., Simpson, J., Kane, A., Menon, D., Nori, A., Criminisi, A., Rueckert, D., Glocker, B.: Unsupervised domain adaptation in brain lesion segmentation with adversarial networks. In: Niethammer, M., Styner, M., Aylward, S., Zhu, H., Oguz, I., Yap, P.T., Shen, D. (eds.) *Information Processing in Medical Imaging*. pp. 597–609. Springer International Publishing, Cham (2017)
9. Liu, Z., Mao, H., Wu, C.Y., Feichtenhofer, C., Darrell, T., Xie, S.: A convnet for the 2020s. Proceedings of the IEEE/CVF Conference on Computer Vision and Pattern Recognition (CVPR) (2022)
10. Ma, J., He, Y., Li, F., Han, L., You, C., Wang, B.: Segment anything in medical images. *Nature Communications* **15**, 654 (2024), <https://www.nature.com/articles/s41467-024-44824-z>
11. Moccia, S., De Momi, E., El Hadji, S., Mattos, L.S.: Blood vessel segmentation algorithms — review of methods, datasets and evaluation metrics. *Computer Methods and Programs in Biomedicine* **158**, 71–91 (2018). <https://doi.org/10.1016/j.cmpb.2018.02.001>
12. Mouches, P., Forkert, N.D.: A statistical atlas of cerebral arteries generated using multi-center MRA datasets from healthy subjects. *Scientific Data* **6**, 29 (2019). <https://doi.org/10.1038/s41597-019-0034-5>
13. Ouyang, C., Biffi, C., Chen, C., Kart, T., Qiu, H., Rueckert, D.: Self-supervision with superpixels: Training few-shot medical image segmentation without annotation. In: European conference on computer vision. pp. 762–780. Springer (2020)
14. Phellan, R., Peixinho, A., Falcão, A., Forkert, N.D.: Vascular segmentation in TOF MRA images of the brain using a deep convolutional neural network. In: *Intravascular Imaging and Computer Assisted Stenting, and Large-Scale Annotation of*

- Biomedical Data and Expert Label Synthesis. pp. 39–46. Springer International Publishing, Cham (2017). https://doi.org/10.1007/978-3-319-67534-3_5
15. Shit, S., Paetzold, J.C., Sekuboyina, A., Ezhov, I., Unger, A., Zhylka, A., Plum, J.P., Bauer, U., Menze, B.H.: cldice-a novel topology-preserving loss function for tubular structure segmentation. In: Proceedings of the IEEE/CVF Conference on Computer Vision and Pattern Recognition. pp. 16560–16569 (2021)
 16. Siméoni, O., Vo, H.V., Seitzer, M., Baldassarre, F., Oquab, M., Jose, C., Khalidov, V., Szafraniec, M., Yi, S., Ramamonjisoa, M., et al.: Dinov3. arXiv preprint arXiv:2508.10104 (2025), <https://arxiv.org/abs/2508.10104>
 17. Su, J., Lu, Y., Pan, S., Murtadha, A., Wen, B., Liu, Y.: Roformer: Enhanced transformer with rotary position embedding. *Neurocomputing* **568**, 127063 (2024)
 18. Tajbakhsh, N., Jeyaseelan, L., Li, Q., Chiang, J.N., Wu, Z., Ding, X.: Embracing imperfect datasets: A review of deep learning solutions for medical image segmentation. *Medical Image Analysis* **63**, 101693 (2020), <https://doi.org/10.1016/j.media.2020.101693>
 19. Tetteh, G., Efremov, V., Forkert, N.D., Schneider, M., Kirschke, J., Weber, B., Zimmer, C., Piraud, M., Menze, B.H.: Deepvesselnet: Vessel segmentation, centerline prediction, and bifurcation detection in 3-d angiographic volumes. *Frontiers in Neuroscience* **14** (2020). <https://doi.org/10.3389/fnins.2020.592352>
 20. Wang, H., Guo, S., Ye, J., Deng, Z., Cheng, J., Li, T., Chen, J., Su, Y., Huang, Z., Shen, Y., Fu, B., Zhang, S., He, J., Qiao, Y.: Sam-med3d: Towards general-purpose segmentation models for volumetric medical images (2024), <https://arxiv.org/abs/2310.15161>
 21. Wang, J., Chen, M., Karaev, N., Vedaldi, A., Rupprecht, C., Novotny, D.: Vggt: Visual geometry grounded transformer. In: Proceedings of the IEEE/CVF Conference on Computer Vision and Pattern Recognition (2025)
 22. Yang, K., Musio, F., Ma, Y., et al.: Benchmarking the CoW with the TopCoW challenge: Topology-aware anatomical segmentation of the circle of willis for CTA and MRA. arXiv preprint arXiv:2312.17670 (2023)
 23. Yoon, J.S., Oh, K., Shin, Y., Mazurowski, M.A., Suk, H.I.: Domain generalization for medical image analysis: A review. *Proceedings of the IEEE* **112**(10), 1583–1609 (2024). <https://doi.org/10.1109/JPROC.2024.3507831>
 24. Zhang, J.O., Sax, A., Zamir, A., Guibas, L., Malik, J.: Side-tuning: A baseline for network adaptation via additive side networks (2020), <https://arxiv.org/abs/1912.13503>